Direct subsurface absorption of hydrogen on Pd(111): Quantum mechanical calculations on a new two-dimensional potential energy surface

R. A. Olsen, P. H. T. Philipsen, and E. J. Baerends
Theoretische Chemie, Vrije Universiteit, De Boelelaan 1083, 1081 HV Amsterdam, The Netherlands

G. J. Kroes
Leiden Institute of Chemistry, Gorlaeus Laboratories, Postbus 9502, 2300 RA Leiden, The Netherlands

O. M. Løvvik
University of Oslo, Department of Physics, P.O. Box 1048 Blindern, N–0316 Oslo, Norway

(Received 22 October 1996; accepted 5 March 1997)

We have calculated a two-dimensional (2D) potential energy surface (PES) for H_2 interacting with a Pd(111) surface. The geometry considered is for H_2 approaching a bridge site and dissociating into neighboring hollow sites and the subsurface sites directly below these. Density functional calculations were performed using both the local density approximation (LDA) and the generalized gradient approximation (GGA). The LDA PES gives the usual overbinding and shows no barrier (relative to the bottom of the H_2 potential) to subsurface absorption, while the GGA PES agrees with the experimental adsorption energies and has a large barrier. We have performed quantum mechanical wave packet calculations on the GGA PES to obtain the direct subsurface absorption probability. We have also calculated the barrier height's dependence on a coordinate that can be associated with a local surface vibrational mode and the results suggest that this degree of freedom should be taken into account in the dynamical calculations. © *1997 American Institute of Physics.* [S0021-9606(97)01722-4]

I. INTRODUCTION

The Pd(111) surface is interesting because both experimental[1–7] and theoretical[2,3,8–16] studies show the existence of a hydrogen absorption site located between the first and second metal layer. This so-called subsurface site is energetically more favorable than the bulk site and almost as favorable as the chemisorption site on the surface. Furthermore; Gdowski, Stulen, and Felter[6] claim to have found experimental evidence for hydrogen absorbing directly into the bulk, without equilibrating in the chemisorption well. In Ref. 15 a model PES was constructed to describe a hydrogen molecule dissociatively adsorbing on a Pd(111) surface with the possibilities that the hydrogen atoms either end up in the surface adsorption sites or go directly subsurface. Quantum dynamical calculations were performed on this PES to calculate the probability for direct subsurface absorption. Due to the model character of the PES and the limitations on the number of degrees of freedom considered, no clear conclusion on the possibility for direct subsurface absorption could be drawn. In this study we rectify the first part, presenting a new PES for this system which is based on density functional theory (DFT) within the generalized gradient approximation (GGA). We also present some results for Pd and PdH bulk, investigating the importance of the relativistic corrections for a number of properties. These calculations have helped us to establish which level of theory should be adequate for the calculation of a PES for H_2+Pd(111). Finally, the calculated PES was used in a wave packet study of the dynamics of direct subsurface absorption, the results of which are used to compare with the experimental work of Ref. 6.

The paper is organized as follows. In Section II we give a short description of the BAND program used in our DFT calculations. We also give results for bulk Pd and bulk PdH and compare relativistic and non-relativistic calculations. Section III presents the new PES and Section IV the results of quantum dynamical calculations employing this PES. Section V concludes.

II. ELECTRONIC STRUCTURE CALCULATIONS

A. Method

All the electronic structure calculations presented in this work were performed using BAND.[17,18] This program solves the Kohn–Sham equations[19,20] self-consistently for a periodic system. Bulk calculations are done using full three dimensional translational symmetry, whereas the calculations in Section III employ a semi-infinite slab geometry with translational symmetry in two directions. The one-electron states are either expanded in flexible basis sets of numerical atomic orbitals (NAOs) obtained from numerical Herman–Skillman type calculations,[21] Slater-type orbitals (STOs), or a combination of both. There is no need for pseudopotentials since the frozen core approximation can be used for the core electrons of the heavier atoms. The matrix elements of the Hamiltonian are calculated using an accurate Gauss-type numerical integration scheme,[22] and the **k**-space integration can be done accurately using the quadratic tetrahedron method.[23] No shape approximations are made to the potentials. As shown in Refs. 17 and 18 all the aspects of the numerical integration scheme in BAND, both in real space and **k**-space, are well under control.

TABLE I. The basis sets used in the bulk calculations. A NAO is a numerical atomic orbital obtained from a Herman–Skillman type calculation (Ref. 21). An STO is a Slater-type orbital with the given exponent.

	Pd						H	
	$4s$	$4p$	$4d$	$5s$	$5p$	$4f$	$1s$	$2p$
NAO	yes	yes	yes	yes	no	no	yes	no
STO	3.9	2.7	1.5	1.8	1.8	1.5	1.58	1.0

The exchange-correlation energy in the LDA is calculated using the Vosko–Wilk–Nusair formulas.[24] The GGA we use is the Becke correction[25] for the exchange energy and the Perdew correction[26] for the correlation energy. The gradient correction is calculated from the self-consistent LDA density, which has been shown to be an excellent approximation to the binding energies calculated from the self-consistent nonlocal density.[27] Recently, scalar relativistic corrections introduced through the ZORA-equation[28–30] have been implemented in BAND.

B. Pd bulk

For the calculation of the lattice constant, bulk modulus, and the cohesive energy we only need one Pd atom in our fcc unit cell. This makes the calculations fairly inexpensive and we can achieve a high accuracy in both the real and **k**-space integrations. By performing some test calculations with even higher accuracy, we have found our chosen settings to carry an error of less than 0.03 eV with respect to the numerical integration. The basis set used is a combination of NAOs and STOs and is shown in Table I. The NAOs are generated from the $4d^9 5s^1$ starting configuration we have chosen for the Pd atom. As has been shown in Refs. 17 and 31 this kind of basis set has triple zeta quality. Adding a $5g$ function to the basis set or making small changes to the exponents of the STOs changes the energies by less than 0.02 eV, indicating how close we are to the basis set limit. The frozen core approximation has been used for orbitals up to and including $3d$. All in all our reported values should be very close to the actual values for the LDA and GGA functionals.

We calculate the energies for 15 different lattice constants. They cover a 20% variation around the experimental value and are equally spaced. The theoretical lattice constant, the cohesive energy, and the bulk modulus for the two functionals are found by fitting the 15 values to Murnaghan's equation of state.[32] Two sets of calculations with 15 points each are done; one for the non-relativistic limit, the other including scalar relativistic corrections. The results are given in Table II.

As noted in several previous papers[16,34–38] the non-relativistic LDA performs quite well. It is the level of theory presented in this paper that comes closest to the experimental Pd bulk results. The reason for this is that the well-known overbinding of the LDA here is compensated by neglecting relativistic corrections, as is seen from Table II. For both functionals the lattice constant is contracted by approximately 2% upon including scalar relativistic corrections.

TABLE II. The cohesive energy (E_{coh}), lattice constant (a_{lat}), and bulk modulus (B_0) for Pd from experiments and different levels of theory. The values for the local density approximation (LDA) and the generalized gradient approximation (GGA) are given both in the non-relativistic limit (nr) and including scalar relativistic corrections (sr). The calculated cohesive energy is given with respect to a $4d^{10}5s^0$ Pd atom.

Experiment[a]	E_{coh} [eV/atom] 3.89		a_{lat} [a_0] 7.35		B_0 [Mbar] 1.81	
	nr	sr	nr	sr	nr	sr
LDA	4.01	5.03	7.38	7.26	1.74	2.14
GGA	2.68	3.58	7.63	7.47	1.26	1.58

[a]From Ref. 33.

This is accompanied by an increase of 25%–35% in the cohesive energy and bulk modulus. The GGA performs well compared to experiments when scalar relativistic corrections are taken into account, even though the agreement is not as good as for the non-relativistic LDA. This will change when we study PdH bulk in the following.

C. PdH bulk

The hydrogen basis set is given in Table I. Table III gives the results for the H_2 molecule using this basis set in the two DFT approximations. It is seen that the chosen basis set gives very good agreement with experiments for the GGA functional. Next we place a hydrogen atom in the octahedral site (see Fig. 1) in the Pd fcc unit cell, the site the hydrogen is known to occupy from experiments.[40–43] The energies are then calculated for 15 different lattice constants. As in the Pd bulk calculations they span a 20% range around the experimental value and are equally spaced. A 3rd order polynomial fit is used to determine the minimum. This gives the theoretical lattice constant and the cohesive energy for the two approximations we consider. By subtracting the corresponding Pd cohesive energy from Table II and also subtracting half the binding energy of the H_2 molecule from Table III, we find the absorption energy per hydrogen atom. These results are given in Table IV.

As for Pd bulk, the PdH lattice constant contracts upon including scalar relativistic corrections, even though the correction is a bit smaller (about 1%). The absorption energy also decreases. Again the non-relativistic LDA lattice constant is in very good agreement with experiments, but the absorption energy is far off. As expected the relativistic corrections in the Pd–H bonds are much smaller than in the Pd–Pd bonds. Thus the fortunate cancellation between the

TABLE III. The binding energy (E_{b}), bond length (r_0), and vibrational frequency ($\tilde{\nu}_0$) for the H_2 molecule from experiment and two levels of theory.

Experiment[a]	E_{b} [eV] 4.75	r_0 [a_0] 1.40	$\tilde{\nu}_0$ [cm^{-1}] 4395
LDA	4.84	1.44	4227
GGA	4.80	1.41	4359

[a]From Ref. 39.

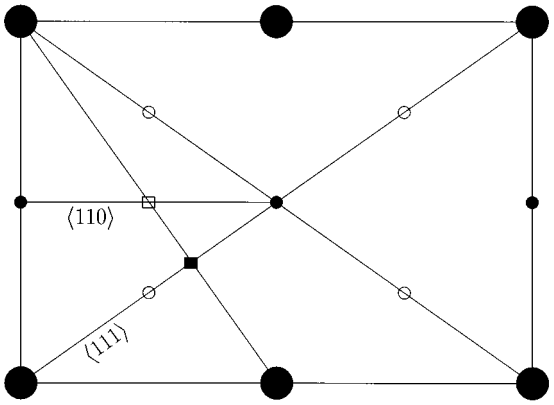

FIG. 1. A (110) plane of the fcc lattice is shown. The large, filled circles are the positions of the Pd atoms, the small, filled circles the octahedral sites, and the small, open circles the tetrahedral sites. The filled square is one of the S_{111} transition states and the open square is one of the S_{110} transition states. Also the two directions ⟨111⟩ and ⟨110⟩ are indicated.

two errors in LDA, the overbinding and neglect of relativistic corrections, is no longer present for the absorption energy. We therefore see the usual overbinding associated with LDA. The non-relativistic GGA seems to give better agreement with experiments for the absorption energy than the scalar relativistic GGA. But before drawing any conclusions we should consider the effect of zero-point energies. The zero-point energy in the octahedral site is about 0.10 eV[44] and 0.13 eV per H atom in the hydrogen molecule. Thus the non-relativistic GGA absorption energy moves to 0.25 eV and the scalar relativistic GGA absorption energy moves to 0.14 eV. Both approximations must therefore be said to give reasonable agreement with the experimental value. Looking at the theoretical lattice constant, the scalar relativistic GGA comes closer to the experimental value than the non-relativistic GGA.

We have also calculated the lattice constant and absorption energy for two hypothetical compounds. The first is PdH with H occupying one of the two tetrahedral sites (see Fig. 1) in the unit cell. The second is PdH_2 with hydrogen in both tetrahedral sites. The results are shown in Table V. We first note that the GGA favors the tetrahedral site in PdH which is at variance with experiments. This we can understand from Table II where we see that the GGA underestimates the bulk modulus of Pd. The GGA therefore underestimates the energy it takes to expand the Pd lattice. Furthermore, the smaller tetrahedral site is expected to have a higher zero-point energy than the larger octahedral site, thus favoring occupation of the octahedral site. The GGA shows PdH_2 to be unstable with respect to H_2 in the gas phase, whereas LDA predicts PdH_2 to be a stable compound which is a result of the usual overbinding. But as noted in Ref. 45, a chemical potential shift could stabilize a PdH_2 phase.

Next we go on to determine the potential barrier to diffusion along two different paths. One is a path where the hydrogen goes directly from one octahedral site to another along the ⟨110⟩ direction and passes what we will call the S_{110} transition state (see Fig. 1). The other is an indirect path from an octahedral to tetrahedral site along the ⟨111⟩ direction and on to another octahedral site. Between the octahedral and tetrahedral site the hydrogen passes the S_{111} transition state. Our reported potential barrier is the absorption energy difference between the transition state and the octahedral site. The results are shown in Table VI. In addition to the values for the experimental lattice constant, values for both the LDA and GGA optimized lattice constant are given. From this three things are clear. Direct diffusion from one octahedral site to another through the S_{110} transition state is hindered by a large barrier. As also concluded by others[14,46–48] the diffusion path goes via the S_{111} transition state and tetrahedral site. Further we see that the two DFT

TABLE IV. The hydrogen absorption energy (E_{abs}) in the octahedral site of Pd and the PdH lattice constant (a_{lat}) from experiments and the two levels of theory. The values for the local density approximation (LDA) and the generalized gradient approximation (GGA) are given both in the non-relativistic limit (nr) and including scalar relativistic corrections (sr). The absorption energy is found according to $E_{abs}=E_{coh}(PdH)-E_{coh}(Pd)-\frac{1}{2}E_b(H_2)$.

Experiment[a]	E_{abs} [eV/H atom] 0.2		a_{lat} [a_0] 7.73	
	nr	sr	nr	sr
LDA	0.68	0.54	7.73	7.65
GGA	0.22	0.11	7.92	7.82

[a]From Ref. 44.

TABLE V. The hydrogen absorption energy (E_{abs}) and lattice constant (a_{lat}) for PdH with hydrogen in the octahedral site (O), tetrahedral site (T), and for PdH_2 with both hydrogen atoms in the tetrahedral sites (2T). The calculations include scalar relativistic corrections. The absorption energy for O and T are found according to $E_{abs}=E_{coh}(PdH)-E_{coh}(Pd)-\frac{1}{2}E_b(H_2)$ and for 2T according to $2E_{abs}=E_{coh}(PdH_2)-E_{coh}(Pd)-E_b(H_2)$.

	E_{abs} [eV/H atom]			a_{lat} [a_0]		
	PdH (O)	PdH (T)	PdH_2 (2T)	PdH (O)	PdH (T)	PdH_2 (2T)
LDA	0.54	0.52	0.31	7.65	7.84	8.28
GGA	0.11	0.20	−0.05	7.82	8.02	8.45

TABLE VI. The potential barrier (E_{bar}) to diffusion through the two transition states (TS) S_{110} and S_{111}. The values are given for the experimental lattice constant ($a_{lat}=7.73$), the LDA optimized lattice constant ($a_{lat}=7.65$), and the GGA optimized lattice constant ($a_{lat}=7.82$). The calculations include scalar relativistic corrections. The potential barrier is the difference between the adsorption energy of a hydrogen on the given transition state and the absorption energy of a hydrogen in the octahedral site. The activation energy for diffusion in palladium hydride has been measured to be 230–300 meV (Refs. 43,44,49–52).

a_{lat} [a_0]	TS	E_{bar}, LDA [eV]	E_{bar}, GGA [eV]
7.73	S_{110}	1.23	1.19
	S_{111}	0.23	0.22
7.65	S_{110}	1.37	1.33
	S_{111}	0.30	0.28
7.82	S_{110}	1.08	1.04
	S_{111}	0.16	0.15

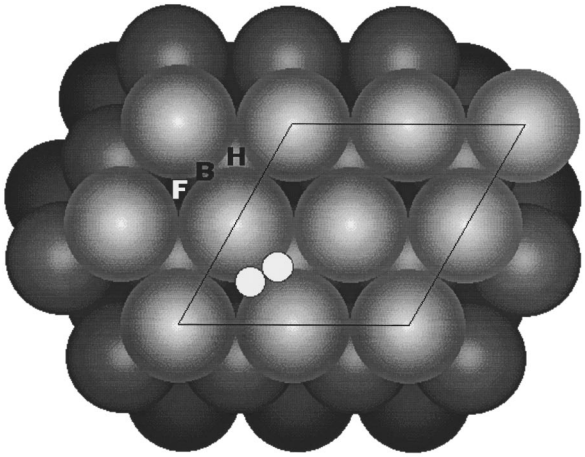

FIG. 2. The slab geometry used in the calculations of the PES. The 2×2 surface unit cell is marked by the solid lines. The two small white discs represent the hydrogen atoms. The bold letters F, B, and H designate the fcc, bridge, and hcp sites, respectively. Directly below the fcc site is in the surface plane the S_{111} transition state, and between the first and second layers the subsurface octahedral site. Directly below the hcp site is in the surface plane another S_{111} transition state, and between the first and second layers the subsurface tetrahedral site.

approximations give almost the same barrier for a chosen lattice constant. Finally, we see that the theoretical barrier is strongly dependent on the chosen lattice constant. We have performed some additional calculations where we change the lattice constant from 7.2 to 8.0 a_0, and we see that the GGA diffusion barrier drops from 0.76 to 0.04 eV (scalar relativistic corrections are included).

From Table VI we see that the theoretical barrier for diffusion through the S_{111} transition state and tetrahedral site compares very favorably with experiments, as the activation energy for diffusion in palladium hydride has been measured to be 230–300 meV.[43,44,49–52]

III. THE DFT PESs FOR H_2/Pd(111)

A. Approximations and convergence

The 2D PES we present here is for H_2 dissociating above a bridge site into the surface threefold hollow sites and the subsurface sites directly below these. This geometry is shown in Fig. 2. The geometry employed allows the atoms to follow the atomic diffusion path in the bulk in the sense that both H atoms can pass the S_{111} transition states on the way to the subsurface sites. The two degrees of freedom treated are the hydrogen molecule's bond distance, r, and the distance of the center of mass to the surface, Z. Z is taken positive above the surface and negative below the surface. The center of mass is always kept above/below the bridge site and the bond axis is kept parallel to the surface plane.

We have chosen a 2×2 surface unit cell to model the dissociation process. Comparison of the binding energy of the hydrogen molecule within a bare 2×2 overlayer and that of a single H_2 molecule shows direct interactions between the molecules to be present only for bond distances larger than 5.5–6.0 a_0. And as is seen from experiments,[53] the adsorption energy remains constant up to about a half monolayer coverage. With our choice of surface unit cell we are therefore describing a dissociation event in the low coverage limit. A similar finding was obtained in a study by Wilke and Scheffler on the analogous $H_2+Pd(100)$ system.[54] Further we have done the calculations on a 3 layer slab with the H_2 on one side. For adsorption geometries only including surface sites, already a 2 layer slab gives good results.[16,31,55,56] As is seen from Fig. 3 in Ref. 16 the 2 layer calculations also give quite good results for subsurface sites. The same figure also shows that the 3 layer slab gives almost identical results for all adsorption geometries compared to the 5 layer slab. Our choice of a 3 layer slab should therefore provide fairly accurate results.

The basis set from Table I used in the bulk calculations makes our slab calculations rather expensive. But test calculations on a slab with a $\sqrt{3}\times\sqrt{3}$ surface unit cell and 2 layers show that we can remove some of the Pd basis function without giving up too much in accuracy. Four different Pd basis sets, shown in Table VII, have been used to calculate the adsorption energy for three different geometries. The hydrogen basis functions are the same as in Table I. All the geometries have the hydrogen molecule's center of mass above the bridge site. The first, a, has a 1.55 a_0 H_2 bond length with the center of mass 4.4 a_0 above the surface. The second, b, place both hydrogens on the S_{111} transition states shown in Fig. 2. The third, c, is with one of the hydrogens in the hcp site and the other in the octahedral subsurface site. As is seen from Tables VII and VIII we introduce an error of

TABLE VII. The four Pd basis sets used in the test calculations. STO is a Slater-type orbital with the given exponent. All the four basis sets contain $4s$, $4p$, $4d$, and $5s$ numerical atomic orbitals obtained from a Herman–Skillman type calculation (Ref. 21).

Basis		$4s$	$4p$	$4d$	$5s$	$5p$	$4f$
1	STO	no	no	1.5	1.8	1.8	no
2	STO	3.9	2.7	1.5	1.8	1.8	no
3	STO	no	no	1.5	1.8	1.8	1.5
4	STO	3.9	2.7	1.5	1.8	1.8	1.5

TABLE VIII. The adsorption energy (E_{ads}) on a 2 layer slab with a $\sqrt{3}\times\sqrt{3}$ surface unit cell. The basis sets are given in Table VII and the H positions in the text. The adsorption energy is relative to two free hydrogen atoms and a bare Pd slab.

H positions	Basis	E_{ads}, LDA [eV]	E_{ads}, GGA [eV]
a	1	5.11	4.72
	2	5.10	4.72
	3	5.10	4.71
	4	5.10	4.71
b	1	5.57	4.31
	2	5.60	4.34
	3	5.60	4.32
	4	5.63	4.36
c	1	6.19	4.99
	2	6.20	5.00
	3	6.21	5.01
	4	6.22	5.02

0.06 eV in the adsorption energy by dropping the $4s$, $4p$, and $4f$ STOs from the bulk basis set. For bulk Pd, this smaller basis set gives a cohesive energy of 3.43 eV, an optimized lattice constant of 7.52 a_0, and a bulk modulus of 1.50 Mbar in the GGA approximation. Comparing these numbers with Table II, we see that the cohesive energy drops by 0.15 eV with the smaller basis set. Thus quantities that depend directly on the total energies are more affected than quantities that depend on differences between them. We also note that the optimized lattice constant changes very little. In our PES calculations we therefore will use the Pd basis set labelled 1 in Table VII.

Two more choices are to be made: Which lattice constant should we use for the slab? And should we include scalar relativistic corrections? As is seen from Table IV the differences between the non-relativistic and scalar relativistic absorption energy are small, only 0.1 eV. But the overall agreement with experiments is better for the scalar relativistic values, especially for the lattice constant and the bulk modulus, as show in Table II and IV. Since there is little or no extra computational effort demanded to include scalar relativistic corrections, this is the level of theory we select. Further we choose to work with the experimental Pd lattice constant, $a_{\mathrm{lat}}=7.35\ a_0$. This will make it easier if other groups using other methods or levels of theory want to compare their results to ours. That this is desirable is clear from the debate over the barrier height in the H_2/Cu(100) system.[31,57,58]

To help the self-consistent convergence the occupation numbers have been found according to a Fermi-function distribution with $k_BT=0.08$ eV. From this the total energies are extrapolated to zero electronic temperature.[59] The real space integration has been carried out with the ''accint'' parameter[17] set to 4.5. This gives an error of about 0.01 eV in the adsorption energy, as has been verified by increasing the ''accint'' for a few typical geometries. The **k**-space integration was done with the ''kspace'' parameter[17] set to 3. This gives 6 symmetry unique points in the irreducible wedge of the first surface Brillouin zone (SBZ). By calculating the adsorption energy for a few typical geometries with the ''kspace'' parameter set to 5, corresponding to 23 symmetry unique points in the SBZ, the largest errors were found to be about 0.06 eV. The low number of points needed in the SBZ to obtain good results is a result of the accurate quadratic tetrahedron method[23] used in the **k**-space integration.

With the parameters used, the energies constituting the PES should be converged to within 0.1 eV of the LDA and GGA limits for the H_2/Pd(111) system.

B. The LDA and GGA PESs for H_2 on Pd(111)

Both PESs were initially calculated with 58 points spanning the region $0.7<r<5.0\ a_0$ and $-2.5<Z<5.0\ a_0$. Bicubic splines were fitted to the points using the E02ZAF, E02DAF, and E02DEF routines in the NAG library. After locating the saddle point 8 more points were added in this region and the splines refitted. The results are shown in Fig. 3. Apart from the entrance channel, the shapes of the PESs

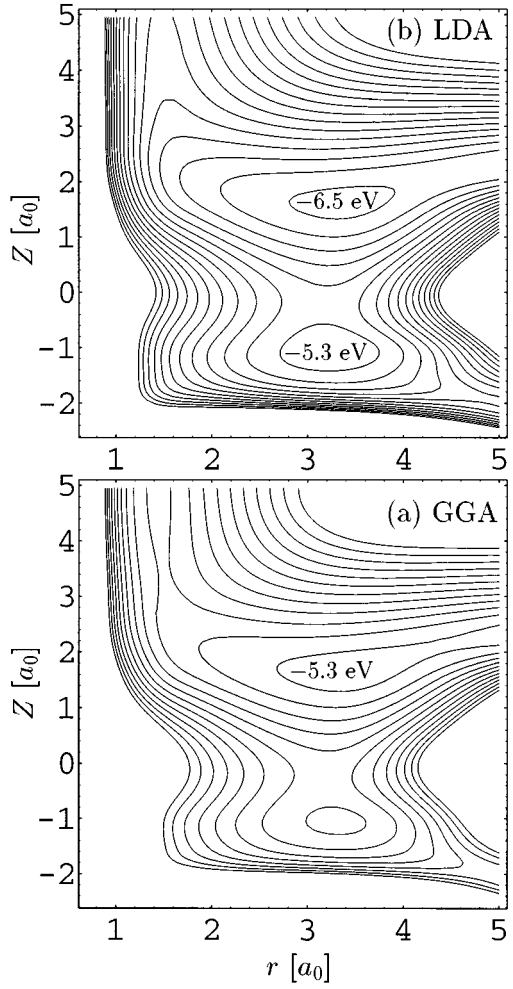

FIG. 3. Contour plots of the GGA (a) and LDA (b) PESs. The contour spacing is 0.3 eV and the energies are relative to two free hydrogen atoms and a bare Pd slab. For the GGA PES the surface minimum lies at $r=3.5$ and $Z=1.7\ a_0$ with a depth of -5.45 eV, the saddle point at $r=3.2$ and $Z=-0.2\ a_0$ with an energy of -3.91 eV, and the subsurface minimum at $r=3.3$ and $Z=-1.1\ a_0$ with a depth of -4.18 eV. For the LDA PES the surface minimum lies at $r=3.4$ and $Z=1.6\ a_0$ with a depth of -6.60 eV, the saddle point at $r=3.2$ and $Z=-0.2\ a_0$ with an energy of -5.21 eV, and the subsurface minimum at $r=3.3$ and $Z=-1.1\ a_0$ with a depth of -5.50 eV.

are similar. Both PESs have the subsurface minimum and saddle point located at $r=3.3$ and $Z=-1.1\ a_0$ and $r=3.2$ and $Z=-0.2\ a_0$, respectively. The depth of the subsurface well is -4.18 eV for the GGA and -5.50 eV for the LDA (measured with respect to two free hydrogen atoms and a bare Pd slab). The corresponding numbers for the saddle point are -3.91 and -5.21 eV. The surface minimum is a bit shifted going from the GGA PES to the LDA PES, but not by much. The GGA surface minimum lies at $r=3.5$ and $Z=1.7\ a_0$ with a depth of -5.45 eV, the LDA minimum at $r=3.4$ and $Z=1.6\ a_0$ with a depth of -6.60 eV. The distance between the hcp and fcc site is 3.0 a_0. Thus the LDA and GGA surface minimum lie very close to a configuration with one H atom in the fcc site and the other in the hcp site. The result of summing the calculated atomic adsorption energy from Ref. 16 for one hcp site and one fcc site makes this

configuration stable by 0.75 eV compared to the bottom of the H_2 potential. In our GGA PES, the adsorption minimum referred to above is stable by only 0.65 eV. The 0.1 eV lower adsorption energy and the larger H_2 bond distance can be understood from the repulsion between the two H atoms (occupying nearest neighbour hcp and fcc sites, the adsorbates come closer together than they would prefer). The theoretical results of Ref. 16 agree well with the experimental results of Refs. 7 and 53, and therefore we conclude that the same holds for our GGA surface minimum. The LDA overbinds as usual, the adsorption minimum being stable by 1.8 eV relative to the bottom of the H_2 potential.

The GGA barrier to direct subsurface absorption lies 0.9 eV above the bottom of the H_2 potential. This barrier has not been directly measured, but we can make a comparison with experiments based on the following arguments. The top of our GGA barrier corresponds to the two hydrogen atoms sitting on two S_{111} transition states in the first Pd layer. We might therefore expect it to be comparable in energy to a configuration with two hydrogen atoms simultaneously occupying two S_{111} transition states in the bulk. We thus need to know the energetic position of this configuration relative to the bottom of the H_2 potential. Using the experimental absorption energy of 0.2 eV per H atom for the hydride,[44] an energy of 0.4 eV is gained in dissociating a hydrogen molecule and putting it inside Pd. The simultaneous diffusion of two H atoms in the hydride is activated by 460–600 meV.[43,44,49–52] Thus the energy needed by a hydrogen molecule to dissociate and push both of its atoms across the bulk diffusion barrier in Pd is about 0.06–0.2 eV, where this number is relative to the ground vibrational state of the molecule. Including the 0.26 eV zero-point energy of the H_2 molecule, this puts the geometry with two H atoms on top of the bulk diffusion barrier about 0.32–0.46 eV higher in energy than the bottom of the H_2 potential. If we compare our 0.9 eV GGA barrier for direct subsurface absorption directly to this number, we find our result to be about 0.5 eV too high.

However, as was seen in Section II C the calculated bulk diffusion barrier was strongly dependent on the chosen lattice constant. This suggests that lattice vibrations play a role in the bulk diffusion process. In comparing our GGA barrier for direct subsurface absorption to experimental values, we should therefore allow for the effects of surface vibrations on the GGA barrier. As is seen from Fig. 4 the GGA barrier depends strongly on a coordinate that can be associated with a local surface vibrational mode. The barrier drops by as much as 0.5 eV for a displacement by 2% of the lattice constant. Including this effect gives a GGA barrier of about 0.4 eV which compares favorably with the 0.32–0.46 eV bulk diffusion barrier we estimated above. We therefore believe that the 0.9 eV GGA barrier for direct subsurface absorption being too high when compared to the bulk diffusion barrier is not due to the GGA approximation, but a result of the reduced dimensionality in our PES.

While the GGA barrier which we have calculated for a static lattice may be correct, the LDA result (about 0.4 eV lower than the bottom of the H_2 potential) should definitely be wrong. This can be attributed to the well-known overbinding of the LDA.

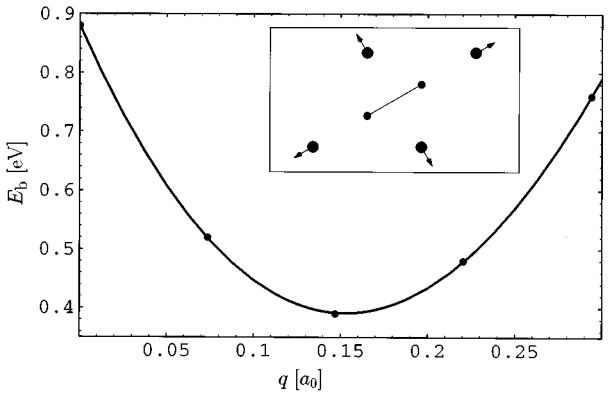

FIG. 4. The dependence of the GGA barrier height (E_B) on a coordinate that can be associated with a local surface vibrational mode. The barrier height is given relative to the bottom of the H_2 potential. The displacement of the Pd atoms in the 2×2 surface unit cell is shown in the inset. All four surface Pd atoms are displaced an equal distance (q). The curve through the data points is meant as a guide for the eye.

The subsurface minimum corresponds to one of the H atoms sitting close to the subsurface tetrahedral site and the other shifted about 1.0 a_0 above the subsurface octahedral site. The LDA value is stable by about 0.7 eV compared to the bottom of the H_2 potential, whereas the GGA is unstable by about 0.6 eV. This indicates a shortcoming of our 2D adsorption/absorption geometries. Experimentally the H atoms on the surface are known to occupy the fcc sites.[7] Restricting ourselves to two degrees of freedom and dissociation above a bridge site means that the two hydrogen atoms move towards different surface sites, the fcc site and the hcp site. This we do not consider a serious shortcoming of our model. After dissociating, enough kinetic energy will be available for the H atoms to move on to other surface sites. But as seen above, restricting both atoms to move subsurface is not very favorable. It would therefore have been desirable to include an angular degree of freedom and allow the possibility of only one hydrogen atom moving subsurface.

Comparing the entrance channel of the GGA and the LDA PES we see a large difference. As is seen from Table III both approximations get the binding energy of the H_2 molecule right. However, the LDA surface minimum is too deep by about 1.1 eV, resulting in a much steeper descent from the gas phase into the surface minimum. The overbinding of the LDA cannot be overcome by a constant shift in the energy: This would result in an erroneous gas phase H_2 potential. The LDA gets the shape of the PES wrong, as is seen even clearer in calculations on $H_2+Cu(100)$[31,57] and on $H_2+Cu(111)$.[27]

We conclude this section with a short remark on what appears to be a barrier in the entrance channel of the GGA PES. The height of this barrier is only about 0.05 eV and below the 0.1 eV accuracy of our calculations. To increase the accuracy to a level needed for determining whether this barrier is real or a result of inaccuracies is at the moment too computationally demanding.

IV. DYNAMICS OF DIRECT SUBSURFACE ABSORPTION

A. Propagation of the wave packet

The 2D Hamiltonian, $\hat{H}$, describing an H_2 molecule dissociating towards the surface hollow sites on a static surface with its center of mass above the bridge site and its axis parallel to the surface plane is given by

$$\hat{H} = -\frac{1}{2M}\frac{\partial^2}{\partial Z^2} - \frac{1}{2\mu}\frac{\partial^2}{\partial r^2} + V(Z,r). \tag{1}$$

The total and reduced mass of the molecule are denoted by M and μ, respectively, and $V(Z,r)$ is the interaction potential, which we will discuss more closely in Section IV C. The initial wave function is chosen to be a product of a vibrational eigenfunction of the hydrogen molecule, $\chi_\nu(r)$, and a superposition of free particle eigenstates in Z,

$$\Psi(Z,r,t_0) = \chi_\nu(r)\int dk_z b(k_z)\frac{1}{\sqrt{2\pi}}\exp(ik_z Z). \tag{2}$$

The momentum distribution function, $b(k_z)$, has a Gaussian shape and is given by

$$b(k_z) = \left(\frac{2\zeta^2}{\pi}\right)^{1/4}\exp[-(k_{z_0}-k_z)^2\zeta^2 + i(k_{z_0}-k_z)Z_0]. \tag{3}$$

This gives an initial wave function centered on Z_0 with its average translational momentum in the Z direction given by k_{z_0}. The width of the momentum distribution is determined by ζ.

The time propagation is done by expanding the time evolution operator according to the Chebyshev technique[60] with a time step of 100 a.u. (2.4 fs). The wave function is represented on a grid spanning the region $-6.0<Z<18.0$ a_0 and $0.2<r<9.2$ a_0 with 320 and 90 points in the Z and r directions, respectively. The kinetic energy part of the Hamiltonian is obtained by the fast Fourier transform (FFT) technique.[61,62] To avoid artificial reflection from the grid boundaries optical potentials have been used to absorb the outgoing wave function. They cover the regions $-6.0<Z<-1.1$ a_0, $12.1<Z<18.0$ a_0, and $5.0<r<9.2$ a_0 and have a quadratic form.[63] The optical potential in the region $-6.0<Z<-1.1$ a_0 is a bit unusual, but it is needed to absorb the outgoing wave function leaving the subsurface region. Additional comments can be found in Section IV C. Further we have kept the grid small in the Z direction by the use of the projection operator formalism of Neuhauser and Baer[64] to bring the initial wave packet in on a separate, one-dimensional grid.

B. Flux analysis

We want to find the probability for the H_2 molecule ending up below the surface. Since there also exists a surface exit channel, the subsurface probability cannot be found by analyzing the wave function reflected back to the gas phase. But the technique of analyzing the flux[65,66] through a cut at a constant value of Z will give us the desired subsurface probability. With this technique we also take advantage of the initial wave function containing a distribution of translational energies in the Z direction.

Integrating the quantum mechanical probability current along a line $Z=Z_{\rm cut}$ and placing this line below the surface give us the probability for going subsurface

$$P = \frac{1}{M}\mathrm{Im}\int dr dt \Psi^*(Z_{\rm cut},r,t)\frac{\partial\Psi}{\partial Z}(Z,r,t)|_{Z=Z_{\rm cut}}. \tag{4}$$

The wave function can at any time be expanded in stationary scattering states[67] as

$$\Psi(Z,r,t) = \int dk_z b(k_z)\exp(-i\hat{H}t)\Psi^+(k_z|Z,r). \tag{5}$$

Inserting Eq. (5) in Eq. (4) and following Ref. 68 we have

$$P = \int dk_z |b(k_z)|^2 P_{\rm e}(k_z), \tag{6}$$

where $P_{\rm e}(k_z)$ is the energy resolved subsurface probability given by

$$P_{\rm e}(k_z) = \frac{2\pi}{|k_z|}\mathrm{Im}\int dr \Psi^{+*}(k_z|Z_{\rm cut},r)\frac{\partial\Psi^+}{\partial Z}(k_z|Z,r)|_{Z=Z_{\rm cut}}. \tag{7}$$

The stationary scattering states and their derivatives are needed in order to calculate the energy resolved subsurface probability in Eq. (7) and are found by inverting Eq. (5) as in Ref. 68,

$$\Psi^+(k_z|Z,r) = \frac{|k_z|}{2\pi M b(k_z)}\int dt\ \exp(iEt)\Psi(Z,r,t), \tag{8a}$$

$$\frac{\partial\Psi^+}{\partial Z}(k_z|Z,r) = \frac{|k_z|}{2\pi M b(k_z)}\int dt\ \exp(iEt)\frac{\partial\Psi}{\partial Z}(Z,r,t). \tag{8b}$$

The way to calculate these scattering states through the Chebyshev expansion is briefly outlined in Ref. 65 and is given a more thorough treatment in Ref. 68. The derivative of the time dependent wave function in Eq. (8b) is obtained by using the FFT technique. It is important to note that the scattering states and their derivatives are not needed on the whole grid. As can be seen from Eq. (7) we only need the values on the line $Z=Z_{\rm cut}$ to obtain the subsurface probability. The integrals over time in Eq. (8) are evaluated using a numerical quadrature with equal spacing, where the time interval used has to be smaller than the time step employed in the Chebyshev expansion. This is straightforward, because results at intermediate times can be obtained using the time dependent Chebyshev coefficients, and hence no extra Hamiltonian operations are required.[68,69]

C. The PES used in the dynamics

From the arguments in Section III B it is clear that the LDA PES does not model the dissociation process very well, thus it is no use employing this PES in the dynamical calculations. On the other hand the GGA PES seems to give a

TABLE IX. The parameters used in the modified Rydberg potential.

D_e [eV]	4.794
r_0 [a_0]	1.410
a_1 [a_0^{-1}]	2.189
a_2 [a_0^{-2}]	1.400
a_3 [a_0^{-3}]	0.688
a_4 [a_0^{-1}]	2.179

good description of a dissociation event, but the spline fitted PES is not defined on a large enough grid to be used in the dynamics. This is easily remedied.

For $Z_{spmax}=5.0\ a_0$ the GGA PES has almost reached the asymptotic values of a free hydrogen molecule. To enable extrapolation to large Z, the gas phase H_2 GGA potential is fitted (in the region $r=0.7-2.9\ a_0$) to a modified Rydberg form

$$V_{H_2}(r)=-D_e\times(1.0+a_1\rho+a_2\rho^2+a_3\rho^3)\exp(-a_4\rho), \tag{9}$$

where $\rho=r-r_0$. The fitting parameters are given in Table IX. At large Z, the spline fitted PES, $V_{spline}(Z,r)$, is then made to go smoothly over into the gas phase H_2 potential by the use of a switching function:

$$V(Z,r)=V_{spline}(Z,r),\quad Z\leqslant Z_{spmax},$$

$$V(Z,r)=f_{switch}(Z)V_{spline}(Z_{spmax},r)+(1-f_{switch}(Z))V_{H_2}(r),$$

$$Z_{spmax}<Z<Z_{spmax}+Z_{switch},$$

$$V(Z,r)=V_{H_2}(r),\quad Z\geqslant Z_{spmax}+Z_{switch}. \tag{10}$$

The switching function is given by

$$f_{switch}(Z)=\frac{1}{2}+\frac{1}{2}\cos(\chi),\quad \chi=\frac{(Z-Z_{spmax})\pi}{Z_{switch}}, \tag{11}$$

where $Z_{switch}=1.75\ a_0$.

From Fig. 3(a) we see that there is no barrierless exit channel from the subsurface minimum. This will result in most of the wave function entering this region being reflected back towards the surface. Since we do not believe this to be a physical effect, but rather a shortcoming of our 2D model, we make the assumption that, once $Z<-1.1\ a_0$, the molecule is absorbed subsurface and can no longer be reflected back to the surface or the gas phase. This is done by making the PES equal to its values along the line $Z=-1.1\ a_0$ for all geometries below this line. Furthermore, as mentioned in Section IV A an optical potential is used in the region $-6.0<Z<-1.1\ a_0$ to absorb the wave function and to avoid it reaching the $Z=-6.0\ a_0$ boundary of the grid.

Physical reasoning can be used to justify the above assumption. After the hydrogen atoms have entered the subsurface region a number of things may happen. The surface might to some extent relax outwards and make the subsurface sites energetically more favorable, as is suggested by the timescale arguments in Ref. 15. The atom above the octahedral site will probably move closer to this site. And it is likely that the hydrogen atom close to the tetrahedral site will use some of its kinetic energy to move on to another octahedral site. To be able to explore the last two possibilities, the hydrogen molecule needs to make use of all its six molecular degrees of freedom. Including an optical potential to absorb the wave function once $Z<-1.1\ a_0$ is thus a way of including the degrees of freedom we neglect, making the assumption that the result of the motion in these degrees of freedom is that the molecule will not be reflected back to the gas phase. A similar assumption is usually made in 2D wave packet calculations on dissociative adsorption, where an optical potential is applied to remove the wave function once it arrives at the first adsorption minimum. This way, any (partial) reflection that might result from further outward motion in r (due to periodic sampling of the less favorable atomic adsorption sites) is neglected.

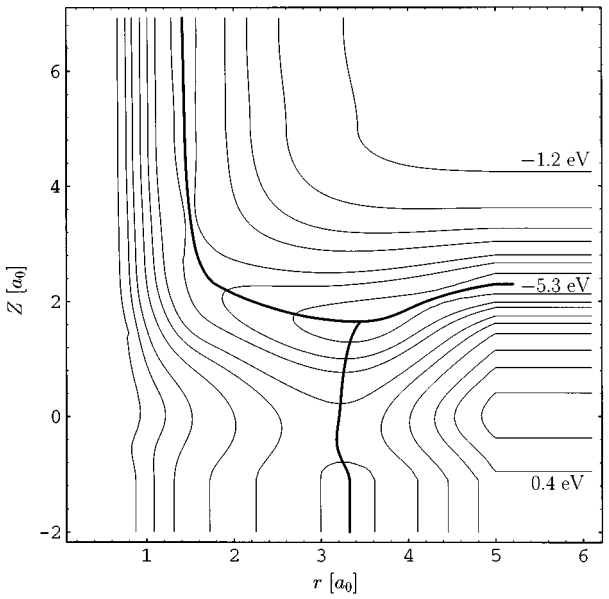

FIG. 5. Contour plot of the GGA PES used in the dynamics. The contours are at − 5.3, − 5.0, − 4.7, − 4.1, − 3.5, − 2.6, − 1.2, 0.4, and 3.4 eV and the energies are relative to two free hydrogen atoms and a bare Pd slab. The thick, solid curve shows the calculated reaction path.

Finally we need the potential for large values of r. In a similar vein as above we choose to make the potential equal to the values on the line $r=5.0\ a_0$ for all geometries with larger values of r.

The resulting PES is shown in Fig. 5. This is the interaction potential, $V(Z,r)$, that goes into the Hamiltonian of Eq. (1). What is important to note is that the barrier region of Fig. 3(a) is unaltered in Fig. 5. The shape and the height of this barrier will be determining the direct subsurface absorption probability.

D. The direct subsurface absorption probability

To obtain results for a large range of translational energies, three separate wave packet calculations were performed for scattering of H_2 in its $\nu=0$ (vibrational ground) state, employing different values k_{Z_0} and ζ. For scattering of H_2 in its $\nu=1$ state four different calculations were done. Each

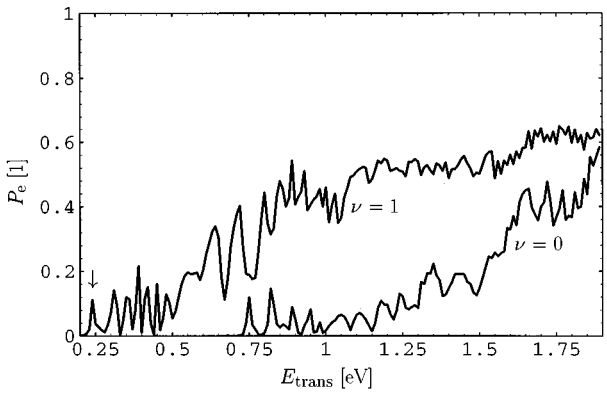

FIG. 6. The direct subsurface probability (P_e) for different initial translational energies (E_{trans}). Results for H_2 in the vibrational ground state ($\nu=0$) and first excited state ($\nu=1$) are shown. The arrow indicates the peak for which the stationary scattering state of Fig. 7 has been plotted.

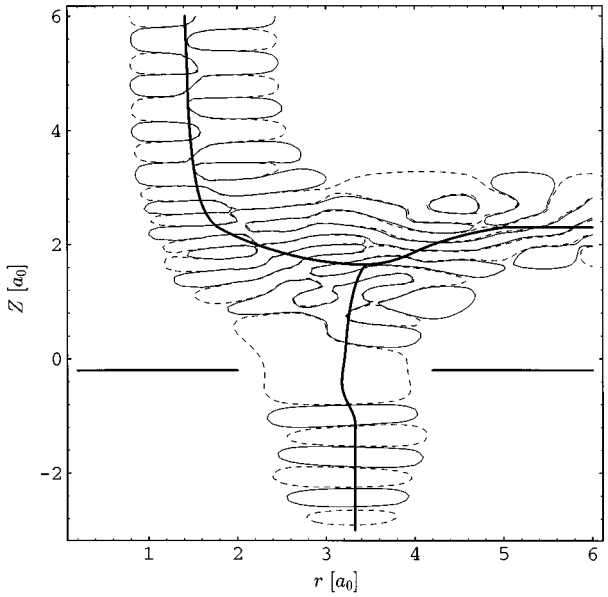

FIG. 7. Contour plot of the real part of the stationary scattering state, $\Psi^+(k_z|Z,r)$. It is plotted for the translational energy $k_z^2/2M=0.24$ eV and $\nu=1$. This corresponds to the first peak in the subsurface absorption probability for the $\nu=1$ curve in Fig. 6. The two straight lines in the plot indicate the position of the top of the barrier, $Z=-0.2$ a_0. Two contour lines are shown in the plot, one for a negative value of the real part of the stationary scattering state (dashed line), the other for the same absolute value, but positive (solid line). The thick, solid curve is the calculated reaction path.

wave packet was propagated for 30 000 a.u. (0.73 ps) with the wave function initially centered on $Z_0=15.0$ a_0. The flux analysis presented in Section IV B was performed with $Z_{cut}=-1.1$ a_0. By changing all parameters that influence the subsurface absorption probability convergence to within a probability of 0.02 was verified. Due to the presence of resonances, which we have not analysed here, a small residual norm was left on the grid after a propagation time of 30 000 a.u. (0.73 ps), but this does not change the results on the accuracy level we report.

The results in Fig. 6 show that the subsurface absorption probability remains negligible until a translational energy of about 0.75 eV for H_2 in its vibrational ground state. The energetic threshold of 0.75 eV is appreciably lower than the barrier of 0.9 eV. This will be explained below. Further we see that the probability shows a lot of structure indicating a rather complicated dynamical picture. Since we only are interested in the possibility for direct subsurface absorption in this study, no attempt has been made to analyze this structure within the framework of resonances. The probability rises slowly with increasing translational energy and does not pass 25% until the collision energy is approximately 1.6 eV.

Exciting the molecular bond by one quantum increases the probability of the hydrogen atoms going subsurface, with the onset of subsurface absorption occurring around 0.24 eV. The downshift of the energetic threshold for the $\nu=1$ curve compared to the $\nu=0$ curve in Fig. 6 corresponds exactly to the 0.51 eV energy of the vibrational quantum. Thus vibrational excitation is very effective in promoting subsurface absorption in this system. For molecular dissociation into surface channels we already know that vibrational excitation can enhance the dissociation probability (see, e.g., Refs. 70, 71 and references therein). In 2D calculations on activated dissociative chemisorption,[72–75] the ideas of a reaction path and vibrational adiabatic potentials have proven to be a convenient tool for explaining this effect. The PES we are considering has two exit channels and is therefore qualitatively different from the so-called elbow potentials, but we will still borrow the main ideas to explain why the energetic threshold is lower than the barrier for the $\nu=0$ curve in Fig. 6 and why vibrational excitation is so efficient in promoting subsurface absorption.

In Fig. 5 the calculated reaction path is shown together with the PES. The ground state vibrational energy associated with the motion perpendicular to the reaction path is 0.26 eV far out in the entrance channel, which is nothing but the zero-point energy of the H_2 molecule. The vibrational energy of the first excited state is 0.77 eV. The two corresponding energies for the motion perpendicular to the reaction path on the top of the barrier are 0.14 and 0.41 eV. Thus the reduction in zero-point energy from 0.26 to 0.14 eV helps to explain why the subsurface absorption begins at 0.75 eV instead of closer to the barrier height value of 0.9 eV for the $\nu=0$ subsurface absorption curve in Fig. 6.

The reduction in the first excited state energy from 0.77 to 0.41 eV is not enough to explain the large shift towards lower translational energies for the $\nu=1$ subsurface absorption curve in Fig. 6. To aid our understanding we have plotted the real part of the stationary scattering state, $\Psi^+(k_z|Z,r)$, responsible for the first peak in this curve in Fig. 7. In this plot we see there is no nodal structure left perpendicular to the reaction path for Z on and below the saddle point. This shows very clearly that the wave packet de-excites to the ground vibrational state upon climbing and passing the barrier. The wave function has thence converted $0.77-0.14=0.63$ eV from vibrational to translational energy and the 0.9 eV barrier is effectively reduced to 0.27 eV, which is very close to the 0.24 eV onset of subsurface ab-

sorption for the $\nu=1$ curve. The large decrease in the energetic threshold for direct subsurface absorption is therefore due to vibrational de-excitation, and not to an adiabatic reduction of the energy of motion perpendicular to the reaction path as the path is climbed.

V. CONCLUSIONS

In the experimental work by Gdowski, Stulen, and Felter[6] on the Pd(111) surface, they claim to find evidence that a hydrogen or deuterium molecule can dissociate and directly absorb into the bulk, without equilibrating in the chemisorption state. Our goal has been to describe this process theoretically. To do this we have used density functional theory (DFT) within both the local density approximation (LDA) and generalized gradient approximation (GGA) to calculate a two-dimensional (2D) potential energy surface (PES) for H_2 on Pd(111). On this PES we have performed quantum mechanical wave packet calculations to find the probability for direct subsurface absorption. Several conclusions can be drawn from this study.

We have seen that the LDA overestimates the binding energy between hydrogen and palladium, both for bulk and surface sites. This overbinding is not present in the H_2 molecule, and therefore the LDA gets the shape of the PES for $H_2+Pd(111)$ wrong. The GGA performs better, as the GGA values for the adsorption and absorption energy and the bulk diffusion barrier compare favorably with experiments. The GGA PES shows a large barrier, about 0.9 eV above the bottom of the H_2 potential, to subsurface penetration. This means direct subsurface absorption does not occur before the translational energy of a H_2 molecule in its ground vibrational state reaches about 0.75 eV. Thus our 2D model cannot account for the experimental evidence for direct subsurface absorption given in Ref. 6. However, we believe that this is not due to the GGA approximation, but a result of the reduced dimensionality of the PES. We have shown that the GGA barrier drops from 0.9 eV above the bottom of the H_2 potential to 0.4 eV when displacing the surface Pd atoms by 2% of the lattice constant. Including in our PES a coordinate that can be associated with a local surface vibrational mode would therefore be desirable. Whether this surface coordinate must be given a full dynamical treatment or can be included through a sudden approximation remains to be seen. Work along these lines is in progress.

Our 2D model restricts the atoms in the hydrogen molecule either both to end up in the surface adsorption sites or both to go subsurface. Lifting this restriction by introducing an angular degree of freedom in the PES would therefore also be interesting. Then the possibility of only one of the atoms in the molecule ending up below the surface could be explored. Preliminary work in this direction suggests that the minimum barrier to direct subsurface absorption would then be less than 0.1 eV.

The quantum mechanical wave packet calculations on the PES showed that vibrationally exciting the H_2 molecule was very effective in promoting direct subsurface absorption. The whole vibrational quantum was made available for climbing the barrier. A plot of the stationary scattering state showed very clearly how the vibrationally excited initial wave function de-excited to the ground vibrational state upon climbing and passing the barrier.

The results of our bulk calculations showed that scalar relativistic corrections are important to the accurate calculation of the cohesive energy and the bulk modulus for Pd. The calculated lattice constant was less influenced by these corrections, changing by only about 2%. The corrections for the hydrogen absorption energy in Pd bulk were also rather small, about 0.1 eV. But because the overall agreement with experiments was better when including scalar relativistic corrections, and these corrections can be computed with little expense, they were included in the calculations of the LDA and GGA 2D PES for H_2 + Pd(111).

ACKNOWLEDGMENTS

The calculations reported here have been carried out under a grant of computer time by the Dutch National Computing Facilities Foundation (NCF). Both R.A.O. and O.M.L. are financed by the Norwegian Research Council. P.H.T.P. was supported by the Netherlands Foundation for Chemical Research (SON), with financial aid from the Netherlands Organization for Scientific Research (NWO). G.J.K. acknowledges financial support by the Royal Netherlands Academy of Arts and Sciences (KNAW).

[1] W. Eberhardt, F. Greuter, and E. W. Plummer, Phys. Rev. Lett. **46**, 1085 (1981).
[2] W. Eberhardt, S. G. Louie, and E. W. Plummer, Phys. Rev. B **28**, 465 (1983).
[3] T. E. Felter, S. M. Foiles, M. S. Daw, and R. H. Stulen, Surf. Sci. Lett. **171**, L379 (1986).
[4] G. D. Kubiak and R. H. Stulen, J. Vac. Sci. Technol. A **4**, 1427 (1986).
[5] G. E. Gdowski, T. E. Felter, and R. H. Stulen, Surf. Sci. **181**, L147 (1987).
[6] G. E. Gdowski, R. H. Stulen, and T. E. Felter, J. Vac. Sci. Technol. A **5**, 1103 (1987).
[7] T. E. Felter, E. C. Sowa, and M. A. van Hove, Phys. Rev. B **40**, 891 (1989).
[8] C. T. Chan and S. G. Louie, Phys. Rev. B **30**, 4153 (1984).
[9] M. S. Daw and S. M. Foiles, Phys. Rev. B **35**, 2128 (1987).
[10] D. L. Lynch, S. W. Rick, M. A. Gomez, B. W. Spath, J. D. Doll, and L. R. Pratt, J. Chem. Phys. **97**, 5177 (1992).
[11] S. W. Rick, D. L. Lynch, and J. D. Doll, J. Chem. Phys. **99**, 8183 (1993).
[12] J. Rogan, M. Lagos, and I. K. Schuller, Surf. Sci. **318**, L1165 (1994).
[13] R. Löber, Ph.D. thesis, Humboldt-University of Berlin, 1995.
[14] R. Löber and D. Hennig, Phys. Rev. B **55**, 4761 (1997).
[15] O. M. Løvvik and R. A. Olsen, J. Chem. Phys. **104**, 4330 (1996).
[16] J. F. Paul and P. Sautet, Phys. Rev. B **53**, 8015 (1996).
[17] G. te Velde, Ph.D. thesis, Vrije Universiteit, Amsterdam, 1990.
[18] G. te Velde and E. J. Baerends, Phys. Rev. B **44**, 7888 (1991).
[19] P. Hohenberg and W. Kohn, Phys. Rev. **136**, B864 (1964).
[20] W. Kohn and L. J. Sham, Phys. Rev. **140**, A1133 (1965).
[21] F. Herman and S. Skillman, *Atomic Structure Calculations* (Prentice-Hall, New Jersey, 1963).
[22] G. te Velde and E. J. Baerends, J. Comput. Phys. **99**, 84 (1992).
[23] G. Wiesenekker, G. te Velde, and E. J. Baerends, J. Phys. C **21**, 4263 (1988).
[24] S. H. Vosko, L. Wilk, and M. Nusair, Can. J. Phys. **58**, 1200 (1980).
[25] A. D. Becke, Phys. Rev. A **38**, 3098 (1988).
[26] J. P. Perdew, Phys. Rev. B **33**, 8822 (1986).
[27] B. Hammer, M. Scheffler, K. W. Jacobsen, and J. K. Nørskov, Phys. Rev. Lett. **73**, 1400 (1994).
[28] E. van Lenthe, Ph.D. thesis, Vrije Universiteit, Amsterdam, 1996.

[29] E. van Lenthe, E. J. Baerends, and J. G. Snijders, J. Chem. Phys. **101**, 9783 (1994).
[30] P. H. T. Philipsen, E. van Lenthe, J. G. Snijders, and E. J. Baerends (in preparation).
[31] G. Wiesenekker, G. J. Kroes, E. J. Baerends, and R. C. Mowrey, J. Chem. Phys. **102**, 3873 (1995).
[32] F. D. Murnaghan, Proc. Nat. Acad. Sci. **3**, 244 (1944).
[33] C. Kittel, *Introduction to Solid State Physics*, 6th ed. (Wiley, New York, 1986).
[34] D. Tománek, Z. Sun, and S. G. Louie, Phys. Rev. B **43**, 4699 (1991).
[35] S. Wilke, D. Hennig, R. Löber, M. Methfessel, and M. Scheffler, Surf. Sci. **307–309**, 76 (1994).
[36] S. Wilke, D. Hennig, and R. Löber, Phys. Rev. B **50**, 2548 (1994).
[37] C. Elsässer, M. Fähnle, L. Schimmele, C. T. Chan, and K. M. Ho, Phys. Rev. B **50**, 5155 (1994).
[38] Y. Wang, S. N. Sun, and M. Y. Chou, Phys. Rev. B **53**, 1 (1996).
[39] B. H. Brandsen and C. J. Joachain, *Physics of Atoms and Molecules* (Longman Scientific & Technical, Essex, England, 1991).
[40] J. E. Worsham, Jr., M. K. Wilkinson, and C. G. Shull, J. Phys. Chem. Solids **3**, 303 (1957).
[41] K. Sköld and G. Nelin, J. Phys. Chem. Solids **28**, 2369 (1967).
[42] J. M. Rowe, J. J. Rush, L. A. de Graf, and G. A. Ferguson, Phys. Rev. Lett. **29**, 1250 (1972).
[43] G. Nelin and K. Sköld, J. Phys. Chem. Solids **36**, 1175 (1975).
[44] *Hydrogen in Metals*, edited by G. Alefeld and J. Völkl (Springer-Verlag, Berlin, 1978).
[45] X. W. Wang, S. G. Louie, and M. L. Cohen, Phys. Rev. B **40**, 5822 (1989).
[46] O. B. Christensen, P. Stoltze, K. W. Jacobsen, and J. K. Nørskov, Phys. Rev. B **41**, 12413 (1990).
[47] C. Elsässer, M. Fähnle, K. M. Ho, and C. T. Chan, Physica B **172**, 217 (1991).
[48] Y. Li and G. Wahnström, Phys. Rev. B **46**, 14528 (1992).
[49] S. Majorowski and B. Baranowski, J. Phys. Chem. Solids **43**, 1119 (1982).
[50] A. H. Verbruggen, C. W. Hagen, and R. Griessen, J. Phys. F: Met. Phys. **14**, 1431 (1984).
[51] H. Kronmüller, G. Higelin, P. Vargas, and R. Lässer, Z. Phys. Chem. N. F. **143**, 161 (1985).
[52] E. Salomons, J. Phys.: Condens. Matter **2**, 845 (1990).
[53] H. Conrad, G. Ertl, and E. E. Latta, Surf. Sci. **41**, 435 (1974).
[54] S. Wilke and M. Scheffler, Phys. Rev. B **53**, 4926 (1996).
[55] G. te Velde and E. J. Baerends, Chem. Phys. **177**, 399 (1993).
[56] P. H. T. Philipsen, G. te Velde, and E. J. Baerends, Chem. Phys. Lett. **226**, 583 (1994).
[57] J. A. White, D. M. Bird, M. C. Payne, and I. Stich, Phys. Rev. Lett. **73**, 1404 (1994).
[58] P. Kratzer, B. Hammer, and J. K. Nørskov, Surf. Sci. **359**, 45 (1996).
[59] M. J. Gillan, J. Phys.: Condens. Matter **1**, 689 (1989).
[60] H. Tal-Ezer and R. Kosloff, J. Chem. Phys. **81**, 3967 (1984).
[61] M. D. Feit, J. A. Fleck, Jr., and A. Steiger, J. Comp. Phys. **47**, 412 (1982).
[62] D. Kosloff and R. Kosloff, J. Comp. Phys. **52**, 35 (1983).
[63] Á. Vibók and G. G. Balint-Kurti, J. Phys. Chem. **96**, 8712 (1992).
[64] D. Neuhauser and M. Baer, J. Chem. Phys. **91**, 4651 (1989).
[65] D. Neuhauser, M. Baer, R. S. Judson, and D. J. Kouri, Comp. Phys. Comm. **63**, 460 (1991).
[66] D. H. Zhang and J. Z. H. Zhang, J. Chem. Phys. **101**, 1146 (1994).
[67] J. R. Taylor, *Scattering Theory* (Wiley, New York, 1972).
[68] R. C. Mowrey and G. J. Kroes, J. Chem. Phys. **103**, 1216 (1995).
[69] R. Kosloff, J. Phys. Chem. **92**, 2087 (1988).
[70] G. R. Darling and S. Holloway, Surf. Sci. Lett. **268**, L305 (1992).
[71] A. Gross and M. Scheffler, Chem. Phys. Lett. **256**, 417 (1996).
[72] D. Halstead and S. Holloway, J. Chem. Phys. **93**, 2859 (1990).
[73] S. Küchenhoff, W. Brenig, and Y. Chiba, Surf. Sci. **245**, 389 (1991).
[74] G. R. Darling and S. Holloway, J. Chem. Phys. **97**, 734 (1992).
[75] M. Hand and S. Holloway, J. Chem. Phys. **91**, 7209 (1989).